Journal of Catalysis **188,** 132–139 (1999)
Article ID jcat.1999.2643, available online at http://www.idealibrary.com on IDEAL®

Isotopic Studies of Methane Oxidation Pathways on PdO Catalysts

Jacky Au-Yeung, Kaidong Chen, Alexis T. Bell,[1] and Enrique Iglesia[1]

Department of Chemical Engineering, University of California at Berkeley, and Chemical and Materials Sciences Division, E.O. Lawrence Berkeley National Laboratory, Berkeley, California 94720-1462

Received March 18, 1999; accepted June 29, 1999

Mechanistic details of CH_4 oxidation were examined on PdO/ZrO_2 catalysts using isotopic tracer methods and measurements of kinetic isotope effects. Normal kinetic isotope effects were observed using CH_4/O_2 and CD_4/O_2 reactant mixtures. The (k_H/k_D) ratio was between 2.6 and 2.5, and it decreased slightly as the reaction temperature increased from 527 to 586 K. These kinetic isotope effects reflect a combination of kinetic and thermodynamic effects, and the measured values are consistent with rate-determining C–H bond activation steps on surfaces predominantly covered with OH groups. Isotopic equilibration rates for $CH_4/CD_4/O_2$ mixtures were much lower than methane combustion rates, suggesting that C–H bond activation steps are irreversible on PdO at 473–600 K. Reactions of $CH_4/^{18}O_2$ mixtures on $Pd^{16}O$–$Zr^{16}O_2$ led to the initial formation of $C^{16}O_2$, followed by a gradual increase in the concentration of other CO_2 isotopomers as lattice ^{16}O atoms are replaced by ^{18}O from $^{18}O_2$. The involvement of lattice oxygens in C–H bond activation steps is consistent with a Mars–van Krevelen redox mechanism. Reactions of $CH_4/^{16}O_2/^{18}O_2$ mixtures lead to all CO_2 isotopomers without the concurrent formation of $^{16}O^{18}O$. Thus, dissociative oxygen chemisorption is also irreversible during methane combustion. Oxygen atoms in $C^{16}O_2$ exchange with $Pd^{18}O$–$Zr^{18}O_2$ catalysts at temperatures lower than those required for methane combustion, suggesting that CO_2 desorption is quasi-equilibrated. These mechanistic conclusions are consistent with the measured dependence of CH_4 oxidation rates on O_2, CH_4, H_2O, and CO_2 concentrations. The resemblance between the reaction kinetics on PdO/ZrO_2 and on other supported PdO catalysts suggests that the mechanistic conclusions reached in this study are generally valid for methane combustion catalysts based on PdO.

1. INTRODUCTION

Traces of methane are present in the untreated exhaust of automobiles and gas turbines fueled by natural gas. Methane removal via catalytic combustion requires the complete conversion of low methane concentrations (<1000 ppm) to CO_2 and H_2O at the temperatures of effluent streams. Also, low temperatures are required for the ignition of catalytic combustors used to reduce NO_x emissions in power generation turbines. Catalytic combustion of methane occurs on metal oxides without side reactions. Catalysts based on supported PdO clusters are among the most active for methane combustion at low temperatures (1–3).

At low temperatures (<600 K), methane oxidation rates on PdO are proportional to CH_4 concentration, independent of O_2 concentration, and inversely proportional to the concentration of H_2O (2–3). Rates also show a negative second-order dependence on CO_2 when CO_2 concentrations significantly exceed the concentration of H_2O (2). A sequence of elementary steps consistent with these data has been proposed recently (3). The mechanism includes irreversible C–H bond activation on vacancy-oxygen site pairs and quasi-equilibrated desorption of CO_2 and H_2O. The measured rate expression cannot distinguish between quasi-equilibrated and irreversible O_2 chemisorption, because this step is not kinetically significant when OH groups are the most abundant reactive intermediates (MARI). A simple Langmuir–Hinshelwood kinetic equation based on the proposed sequence of elementary steps accurately describes the measured rate expression (3).

In this study, the details of the proposed mechanism were confirmed by measuring kinetic isotope effects (CH_4/CD_4) and the reversibility of the proposed steps. Predeuterated methane and $^{18}O_2$ were used in isotopic equilibration studies during CH_4 oxidation in order to establish the identity and reversibility of each proposed elementary step.

2. EXPERIMENTAL

A PdO/ZrO_2 catalyst was prepared by incipient-wetness. ZrO_2 (RC-100P, Daichi Kigenso Kagaku Kogyo Co.) supports were heated in ambient air from room temperature to 1073 K at a rate of 0.33 K s^{-1}, held at 1073 K for 24 h, and then cooled to room temperature. The surface area measured by N_2 physisorption at its boiling point was 16–25 m^2/g. ZrO_2 was then impregnated to incipient wetness with an aqueous solution of $Pd(NO_3)_2$ (10 wt% Pd; 10 wt% nitric acid, Aldrich) and dried in ambient air for 1–2 h at room temperature (RT). The catalyst was heated from RT to 523 K in dry air at 0.0083 K s^{-1} in order to decompose

[1] To whom correspondence should be addressed. E-mail: iglesia@cchem.berkeley.edu.

0021-9517/99 $30.00

$Pd(NO_3)_2$ slowly. The temperature was then increased at 0.17 K s^{-1} to 773 K and held for 10 h. The Pd concentration was measured by atomic absorption (7.9 wt% Pd).

All catalytic measurements were carried out using a temperature-controlled flow reactor. The tubular reactor is 25 cm long with an inner diameter of 0.4 cm at both inlet and outlet. The center section is 0.8 cm in diameter and contains a porous quartz disk. Gas flow rates were metered by electronic flow controllers (FC-280, RO-28, Tylan). A quadrupole mass spectrometer (Model 100C, UTI) was used in order to measure the chemical and isotopic composition of the reactor effluent.

Pd dispersion was measured by H_2–O_2 titration at 373 K (4). The catalyst was first reduced at 373 K in a mixture of 25% H_2 (99.9% purity, Airco) in He (UHP Grade, Middleton Bay Airgas) flowing at 0.33 cm^3 s^{-1}. The sample was then flushed with pure He for 0.5 h, and the gas stream was switched to 20% O_2/He (Middleton Bay Airgas). At 373 K, a monolayer of chemisorbed oxygen forms on Pd metal at O_2 pressures below 46.7 kPa (4). Finally, H_2 pulses (0.4 cm^3) were introduced in order to titrate chemisorbed oxygen until H_2 concentrations reached a constant value. Based on the reported titration stoichiometries (4)

$$\text{Oxidation:}\quad Pd_{(s)} + 1/2\,O_{2(g)} \rightarrow PdO_{(s)}$$

$$\text{Reduction:}\quad PdO_{(s)} + 3/2\,H_{2(g)} \rightarrow PdH_{(s)} + H_2O_{(g)},$$

the Pd dispersion was calculated to be 13.5%. If we assume hemispherical crystallites, the corresponding average Pd metal crystallite radius is 6.4 nm.

Isothermal methane oxidation reactions were carried out using a mixture containing 1% CH_4 and 4% O_2 (UHP Grade, Middleton Bay Airgas) in He at 1.7 cm^3 s^{-1} and 373–623 K. Argon (~1 mol%) was used as an internal standard. The catalyst (0.53 g) was first treated in 20% O_2 in He at 673 K for 1 h. The temperature was then decreased to 373 K and the reactant stream was introduced. The catalyst temperature was increased to 623 K at a rate of 0.17 K s^{-1}, and methane oxidation rates were obtained by measuring CH_4 and CO_2 concentrations in the effluent using mass spectrometry. The experiment was repeated using CD_4 reactants in order to measure kinetic isotope effects for methane oxidation on PdO/ZrO_2.

H–D isotopic equilibration rates were measured for CH_4/CD_4 mixtures in order to determine the reversibility of C–H bond activation steps. These measurements were carried out using 0.5% CH_4, 0.5% CD_4 (99.9% purity, Isotec), 4% O_2, and He balance at a flow rate of 1.7 cm^3 s^{-1} between 473 and 623 K. The catalyst was pretreated as described above. A trap filled with ~10 g Drierite ($CaSO_4$) was placed after the reactor in order to remove water from the reaction products before mass spectrometric analysis. This was required in order to avoid interference between cracking fragments of H_2O, HDO, and D_2O and those of deuterated methane isotopomers. Mass intensities at 15, 17, 18, 19, and 20 amu for $CH_{4-x}D_x$ and at 40 amu for Ar were used to determine methane isotopomer concentrations. Mass 16 was not used because it contains fragments from O_2 and CO_2.

Mass fragmentation patterns for each $CH_{4-x}D_x$ isotopomer are required in order to determine isotopomer concentrations in the products formed by isotopic CH_4–CD_4 equilibration. CH_4 and CD_4 fragmentation patterns were measured, and those for the other isotopomers (CH_3D, CH_2D_2, and CHD_3) were calculated using reported methods (5). These patterns were then used along with those for Ar, CH_4, and CD_4 in order to obtain relative isotopomer concentrations using matrix inversion methods.

Isotopic equilibration rates were measured using $^{16}O_2$/$^{18}O_2$/CH_4 reactants (2%/2%/1%; $^{18}O_2$–Isotec, 99% purity; He balance) on (0.53 g) PdO–ZrO_2 at a flow rate of 1.7 cm^3 s^{-1} in order to determine the reversibility of O_2 chemisorption during CH_4 combustion. The catalyst pretreatment and experimental procedures were similar to those described above. Gas-phase concentrations of $^{16}O_2$, $^{18}O^{16}O$, and $^{18}O_2$ (at 32, 34, and 36 amu, respectively) and of $C^{16}O_2$, $C^{16}O^{18}O$, and $C^{18}O_2$ (at 44, 46, and 48 amu, respectively) were measured continuously by mass spectrometry.

Isotopic equilibration rates were measured on $Pd^{18}O$/ZrO_2 catalysts using CH_4/$^{18}O_2$/$C^{16}O_2$ mixtures in order to probe the reversibility of CO_2 desorption. A $Pd^{16}O/Zr^{16}O_2$ catalyst was treated in 20% $^{18}O_2$/He at 673 K for 3 h and then flushed with pure He for 1 h. The temperature was decreased to 373 K, and a reactant mixture consisting of CH_4/$^{18}O_2$/$C^{16}O_2$ (4%/1%/0.25% mol) in He was introduced at 1.7 cm^3 s^{-1}. The temperature was then increased from 373 to 623 K at 0.17 K s^{-1} and the gas-phase concentrations of $^{16}O_2$, $^{18}O^{16}O$, $^{18}O_2$, $C^{16}O_2$, $C^{16}O^{18}O$, and $C^{18}O_2$ in the effluent stream were measured continuously by mass spectrometry. The reversibility of CO_2 desorption was determined from the concentration of $C^{16}O^{18}O$ in the effluent stream.

3. RESULTS AND DISCUSSION

The concentration of methane oxidation products (CO_2, H_2O) was measured on PdO/ZrO_2 between 473 and 623 K. Both CH_4 and CD_4 were converted completely at temperatures above 623 K, but CD_4 combustion rates were lower than CH_4 combustion rates at all lower temperatures. Using the kinetic rate equation proposed earlier for methane combustion on similar PdO/ZrO_2 catalysts (3) and the assumption of a plug-flow reactor, the measured rate constant can be expressed by

$$k_{\text{eff}} = \frac{2F_{CH_4}}{n_s}\left(\ln\frac{1}{1-x} - x\right), \qquad [1]$$

in which F_{CH_4}, x, and k_{eff} represent the inlet methane molar flow rate, the methane conversion, and the effective rate

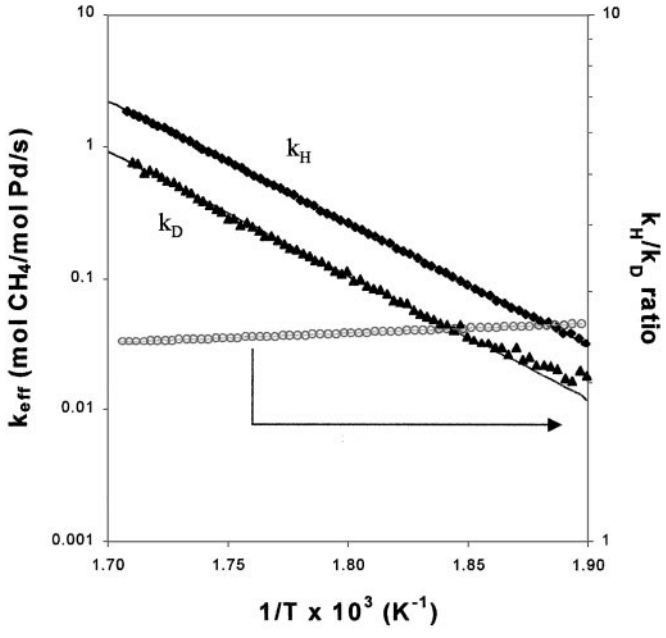

FIG. 1. CH_4 and CD_4 combustion rates and measured kinetic isotope effects on PdO/ZrO_2 (1% CH_4 or CD_4, 4% O_2/He; 100 cm^3/min; 0.53 g 7.9 wt% PdO/ZrO_2).

coefficient, respectively, and n_s is the number of Pd surface atoms. This expression allows the calculation of the reaction rate (k_{eff}) constant from integral reaction rates measured in a plug-flow reactor.

A semilogarithmic plot of k_{eff} as a function of inverse temperature is shown in Fig. 1. A least-square fit to these data between 536 and 586 K was used to determine activation energies. The activation energies for CH_4 and CD_4 oxidation reactions were 176 and 180 kJ/mol, respectively.

The values of k_{eff} determined for CH_4–O_2 and CD_4–O_2 mixtures are denoted as k_H and k_D, respectively, in Fig. 1. The kinetic isotope effect (k_H/k_D) is greater than unity at all temperatures and it decreases slightly with increasing temperature. At 573 K, the kinetic isotope effect is 2.4 while a theoretical treatment using partition functions predicts a value of 2.5 (see Appendix). The observation of a normal isotope effect ($k_H/k_D > 1$) suggests that rate-determining steps in the catalytic sequence involve H-atoms. In the mechanism proposed by Fujimoto *et al.* (3), there are only two elementary steps that involve H atoms, the activation of the C–H bond in CH_4 and the formation of water via recombination of hydroxyl groups. A more detailed discussion of these kinetic isotope effects is presented below and the detailed calculations are included in the Appendix.

The distribution of $CH_{4-x}D_x$ isotopomers formed during oxidation of $CH_4/CD_4/O_2$ reactant mixtures is shown as a function of temperature in Fig. 2. Also shown for comparison is the concentration of the CO_2 formed in methane conversion reactions. The concentration of CO_2 in the effluent stream is also shown in Fig. 2 in order to compare the rate of CH_4/CD_4 isotopic scrambling with methane combustion rates. CH_4/CD_4 equilibration rates, defined as the sum of the rates of CH_3D, CH_2D_2, and CHD_3 formation, remained almost constant at about 1×10^{-3} s^{-1} below 573 K. Above 573 K, the concentrations of all $CH_{4-x}D_x$ isotopomers decreased as a consequence of their conversion to CO_2. The rate of isotopic CH_4–CD_4 equilibration was much smaller than the rate of methane combustion. At 573 K, the isotopic exchange rate is 1.0×10^{-3} s^{-1} and the methane combustion rate is 9.5×10^{-3} s^{-1}. Therefore, C–H bond activation is irreversible during CH_4 combustion on PdO_x-based catalysts at 573 K.

Isotopic scrambling rates for $^{16}O_2/^{18}O_2$ mixtures were also measured during CH_4 oxidation. Figure 3 shows Arrhenius plots for the molar rates of $^{16}O_2$, $^{16}O^{18}O$, and $^{18}O_2$ and of each CO_2 isotopomer exiting the reactor. $C^{16}O_2$ is the first CO_2 isotopomer formed as methane combustion reactions begin to occur above 473 K (Fig. 3), suggesting that lattice ^{16}O in PdO is used more efficiently than oxygen atoms from O_2 in methane combustion. As $C^{16}O_2$ desorbs from the catalytic surface, the resulting oxygen vacancies chemisorb $^{16}O_2$ and $^{18}O_2$ from the gas phase, leading to isotopically mixed oxygen atoms in the lattice and to the formation of all CO_2 isotopomers. Even at the highest temperature (625 K), equilibration of CO_2 isotopomers is incomplete and the equilibrium $C^{16}O_2 : C^{16}O^{18}O : C^{18}O_2$ composition (1 : 2 : 1) is not reached. The higher than equilibrium ^{16}O content in the CO_2 isotopomers shows that the $Pd^{16}O$ starting material retains an excess of ^{16}O at the end of these experiments.

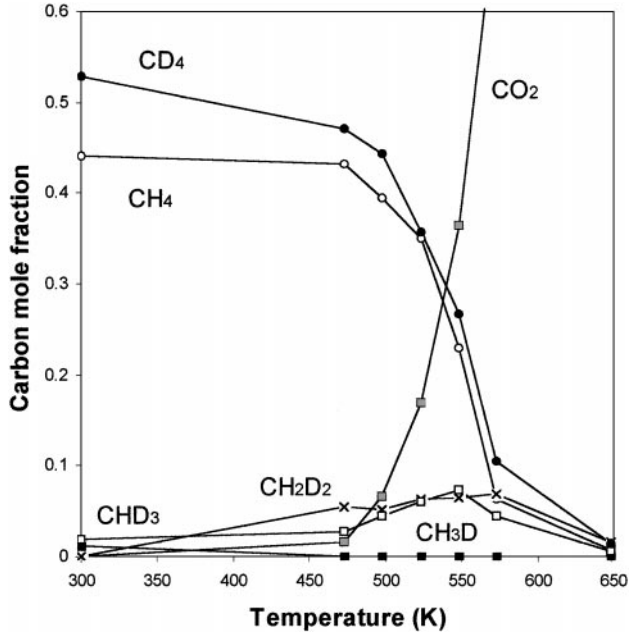

FIG. 2. Methane isotopomer distribution formed during reactions of CH_4–CD_4–O_2 mixtures on PdO/ZrO_2 (0.5% CH_4, 0.5% CD_4, 4% O_2, 1% Ar in He flowing at 100 cm^3/min; 0.52 g 7.9 wt% Pd/ZrO_2).

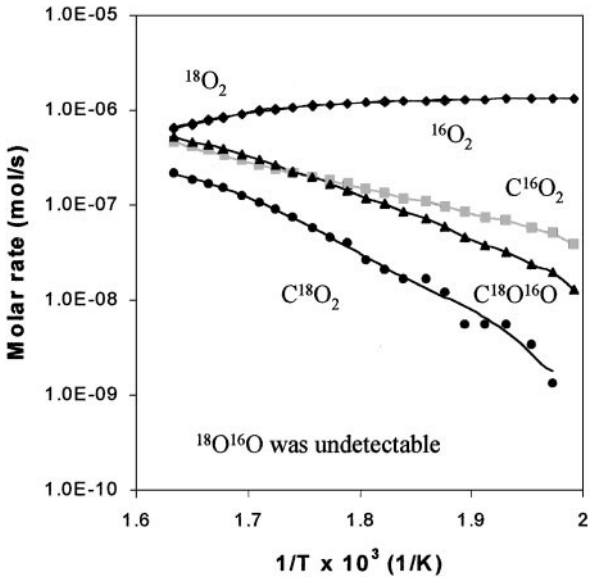

FIG. 3. Oxygen and carbon dioxide isotopomer distributions formed in reactions of CH_4–$^{18}O_2$–$^{16}O_2$ mixtures on PdO/ZrO_2 (2% $^{16}O_2$, 2% $^{18}O_2$, and 1% CH_4 in He flowing at 100 cm^3/min; 0.52 g 7.9 wt% Pd/ZrO_2).

$C^{16}O^{18}O$ is formed at significant rates during reactions of $CH_4/^{16}O_2/^{18}O_2$ mixtures, but $^{16}O^{18}O$ was not detected even at 625 K. These results differ from those obtained during isotopic equilibration of $^{16}O_2/^{18}O_2$ mixtures in the absence of CH_4 (10). Without CH_4, $^{16}O^{18}O$ isotopomers were detected at 575 K when $Pd^{16}O/ZrO_2$ was contacted with a $^{16}O_2/^{18}O_2$ mixture. These results indicate that the rate of recombination of oxygen atoms on PdO surfaces is much slower than the rate at which such oxygen atoms react with methane to form CO_2. An alternate explanation is that the most abundant reactive intermediates (MARI) during CH_4 combustion are surface hydroxyls (3), which recombine to give water in quasi-equilibrated desorption steps. As a consequence, the concentration of surface lattice oxygens is much lower during methane combustion than under the conditions of chemical adsorption–desorption equilibrium prevalent during isotopic scrambling of $^{18}O_2$–$^{16}O_2$ in the absence of CH_4.

The reversibility of CO_2 desorption was established by labeling PdO with ^{18}O, and then contacting the $Pd^{18}O$ formed with a reactant stream containing $^{18}O_2$, CH_4, and $C^{16}O_2$. The formation of $C^{16}O^{18}O$ would require reversible CO_2 desorption steps, because $C^{16}O_2$ is the only source of ^{16}O in the reactant stream. The rates of formation of CO_2 and of its various isotopomers are shown as a function of temperature in Fig. 4. $C^{16}O_2$ in the feed exchanges with $Pd^{18}O$ below 400 K. The concentration of $C^{16}O^{18}O$ increases up to 475 K, at which point the $C^{18}O_2$ formed by methane combustion begins to contribute significantly to the CO_2 molecules present in the gas phase. The exchange of oxygen atoms between $C^{16}O_2$ and $Pd^{18}O$ at temperatures well below those required for combustion shows that CO_2 adsorption–desorption steps are quasi-equilibrated during methane oxidation throughout the entire temperature range of this study.

The results of this study are consistent with the Mars–van Krevelen mechanism (11) proposed by Fujimoto *et al.* (3) for methane combustion on PdO/ZrO_2. The proposed mechanism (Steps 1–7) is consistent with the dependence of methane combustion rates on CH_4, O_2, H_2O, and CO_2 reported by Ribeiro *et al.* (2) and Fujimoto *et al.* (3), when surface hydroxyls are assumed to be the most abundant reaction intermediates (MARI).

$$O_2 + * \overset{K_1}{\rightleftharpoons} O_2^* \qquad \text{Step 1}$$

$$O_2^* + * \xrightarrow{k_2} 2\,O^* \qquad \text{Step 2}$$

$$CH_4 + * \overset{K_3}{\rightleftharpoons} CH_4^* \qquad \text{Step 3}$$

$$CH_4^* + O^* \xrightarrow{k_4} CH_3^* + OH^*$$

$$\rightrightarrows CO_2^*, CO_3^* + \cdots \qquad \text{Step 4}$$

$$2\,OH^* \overset{K_5}{\rightleftharpoons} H_2O + O^* + * \qquad \text{Step 5}$$

$$CO_2^* \overset{K_6}{\rightleftharpoons} CO_2 + * \qquad \text{Step 6}$$

$$CO_3^* \overset{K_7}{\rightleftharpoons} CO_2 + O^* \qquad \text{Step 7}$$

As discussed in detail below, the first steps in the mechanism are the molecular adsorption of O_2 and its subsequent dissociation to O atoms (Steps 1 and 2). The second step is assumed to be irreversible. Neither the kinetic rate

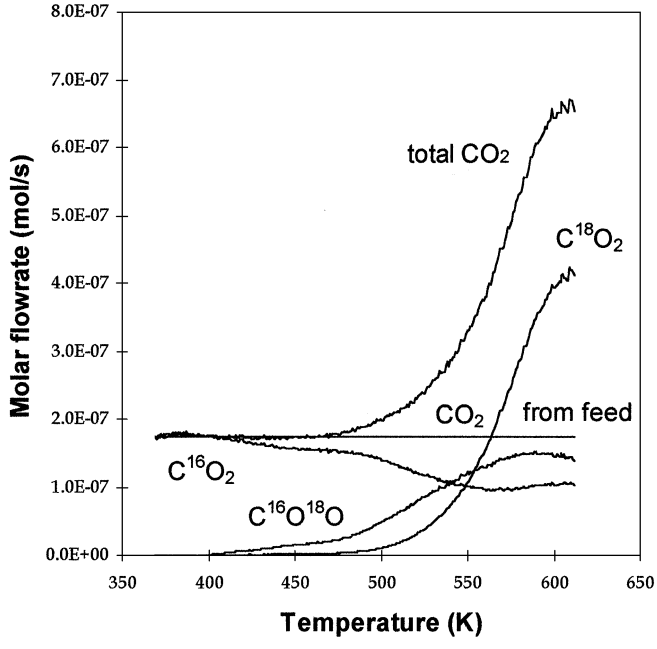

FIG. 4. Carbon dioxide isotopomers formed in reactions of CH_4–$^{18}O_2$–$C^{16}O_2$ mixtures on $Pd^{18}O_2/ZrO_2$ (4% $^{18}O_2$, 1% CH_4, and 0.25% $C^{16}O_2$ in He flowing at 100 cm^3/min; 0.52 g 7.9 wt% Pd/ZrO_2).

expression nor the results of our isotopic tracer studies can discern whether O_2 dissociation is preceded by quasi-equilibrated molecular adsorption. The absence of $^{16}O^{18}O$ during reactions of CH_4–$^{16}O_2$–$^{18}O_2$ mixtures confirmed that Step 2 is indeed irreversible. C–H bonds in methane are activated in Step 4 using a vacancy-oxygen site pair, following the reversible molecular adsorption of methane in Step 3. The finding that isotopic scrambling rates of CH_4–CD_4–O_2 mixtures were much slower than the rate of chemical conversion to CO_2 confirms the assumption that C–H bond activation (Step 4) is irreversible. Steps after the first C–H bond activation reaction involve sequential reactions of lattice oxygens with CH_x species until CO_2 is formed and desorbed. These steps are not kinetically important because they occur after the first irreversible step and they do not involve the most abundant surface intermediates. Water is proposed to form via recombination of surface hydroxyl groups (Step 5). While isotopic evidence for the reversibility of this step was not obtained in the course of this study, the reported inhibition of combustion rates by water requires that Step 5 be reversible, because otherwise gas-phase water could not affect the composition of surface species or the rate of the reaction. The observed inverse dependence of the rate on water concentration requires that this desorption step be quasi-equilibrated. Steps 6 and 7 in the mechanism are the reversible desorption of CO_2 adsorbed on vacant sites or lattice oxygen atoms. The rapid exchange of $C^{16}O_2$ with $Pd^{18}O$ during CH_4 combustion confirmed that Step 7 is quasi-equilibrated.

Applying the pseudo-steady-state approximation to Steps 1 through 7 leads to a Langmuir–Hinshelwood-type kinetic expression.

$$\text{rate} = \frac{K_1 k_2 P_{O_2}}{3\left(1 + \frac{K_1 k_2 P_{O_2}}{3K_3 k_4 P_{CH_4}} + K_1 P_{O_2} + K_3 P_{CH_4} + \left(\frac{K_1 k_2 [H_2O] P_{O_2}}{3K_3 k_4 K_5 P_{CH_4}}\right)^{1/2} + \frac{P_{CO_2}}{K_6} + \frac{K_1 k_2 P_{CO_2} P_{O_2}}{3K_7 K_3 k_4 P_{CH_4}}\right)^2} \quad [2]$$

When OH^* is the most abundant reactive intermediate (MARI), the term in the denominator containing the water concentration becomes much larger than the others and Eq. [2] reduces to the experimentally observed rate expression (2, 3)

$$r = \frac{K_3 k_4 K_5 P_{CH_4}}{P_{H_2O}} = k_{eff} P_{CH_4} / P_{H_2O}. \quad [3]$$

When CO_2 concentrations become significantly higher than H_2O concentrations, the rate given by Eq. [2] becomes proportional to $(P_{CO_2})^{-2}$, as observed experimentally (3). Since H_2O and CO_2 are always formed in a 2 : 1 molar ratio during methane combustion, CO_2 inhibition is unlikely to be observed in practical applications of methane oxidation reactions.

The observed isotopic effects support the above mechanism. The normal isotopic effect suggests either kinetic or thermodynamic relevance elementary steps with the participation of H atoms involved in one reaction cycle. From Eq. [3] one concludes that the rate constant k_{eff} is the combination of the methane adsorption equilibrium constant K_3, the C–H bond dissociation rate constant k_4, and the OH group recombination equilibrium constant K_5; all three steps involve the participation of H atoms. Step 4 is kinetically relevant, and Steps 3 and 5 are thermodynamically relevant. So the isotopic effects obtained reflect the combination of kinetic and thermodynamic effects. A theoretical treatment using partition functions shows that these isotopic effects reflect mainly the difference in zero point energy ($\Delta\varepsilon_0$) between H- and D-containing species; for example, at 573 K, the contribution of the electronic partition function is 2.13, while that from isotopic effects on translational, rotational, and vibrational modes is only 1.19.

4. CONCLUSIONS

A normal kinetic isotope effect was measured for the combustion of methane on Pd/ZrO_2 catalysts. Combustion rates for CD_4/O_2 mixtures are significantly lower than those for CH_4/O_2 reactants. Isotopic equilibration rates in CH_4–CD_4–O_2 are much lower than methane combustion rates. Thus, C–H bond activation steps are irreversible during methane combustion at 523 K on PdO/ZrO_2 catalysts. Isotopic oxygen equilibration was not detected during combustion of $^{16}O_2$–$^{18}O_2$–CH_4 reactant mixtures, showing that dissociative oxygen chemisorption steps are also irreversible. The reversibility of CO_2 desorption steps was confirmed by the rapid scrambling of oxygen atoms between gas-phase $C^{16}O_2$ and lattice oxygens in the $Pd^{18}O$ lattice. These isotopic studies confirm the redox mechanism previously proposed in order to describe the measured dependence of methane oxidation rates on CH_4, O_2, CO_2, and H_2O concentrations (3). In view of the kinetic resemblance among supported PdO methane combustion catalysts, these mechanistic conclusions on PdO/ZrO_2 are likely to apply generally to combustion catalysts based on PdO.

APPENDIX

Theoretical Treatment of the Kinetic Isotope Effect

The appropriate equations for translational, rotational, electronic, and vibrational partition functions at 600 K

are

$$Q_{\text{trans}} = \frac{(2\pi m k_B T)^{3/2} V}{h^3} \propto (mT)^{3/2} \quad [A1.1]$$

$$Q_{\text{rot}} = \frac{8\pi^2}{\sigma h^3}(2\pi k_B T)^{3/2}(I_x I_y I_z)^{1/2} \propto T^{3/2}(I_x I_y I_z)^{1/2} \quad [A1.2]$$

$$Q_{\text{elec}} = g_0 + g_1 e^{-\varepsilon_1/k_b T} + g_2 e^{-\varepsilon_2/k_b T} + \cdots \approx g_0 = e^{-\varepsilon_0/RT} \quad [A1.3]$$

$$Q_{\text{vib}} = \sum_{v=0}^{\infty} e^{-v\theta_v/T} \approx \frac{1}{1-e^{-\theta_v/T}}, \text{ where } \theta_v = \frac{h}{2\pi k_B}\sqrt{\frac{k}{\mu}}. \quad [A1.4]$$

The constants and variables that appear in the equations above are defined as

h	Planck's constant
I_x, I_y, I_z	moment of inertia
k	force constant
k_B	Boltzmann's constant
m	mass of molecules or atoms
T	temperature (K)
V	volume
μ	$m_1 m_2/m_1 + m_2$ = reduced mass
ε_0	zero point energy
σ	symmetry number
θ_v	characteristic temperature for vibration (K)

For gas-phase molecules all four modes of the partition functions are important. However, the translational partition function is always unity for immobile adsorbed species since there are zero degrees of freedom. Values of θ_v are needed to determine the vibrational partition function. Although θ_v for isolated molecules can be found from the literature, values for adsorbed species are scarce. Values of θ_v for isolated molecules in this study are shown in Table A1.1 (12).

Differences in zero point energy ($\Delta\varepsilon_0$) between isotopes are also available from the literature (13). Values of $\Delta\varepsilon_0$ for species encountered in this study are shown in Table A1.2.

For methane combustion, the rate of combustion is proportional to

$$\text{rate} \propto K_3 k_4 K_5. \quad [A1.5]$$

TABLE A1.1

Characteristic Temperature (θ_v) from the Literature

Isolated molecules	θ_v (K) (degeneracy in parentheses)
CH_4	4193, 2196 (2), 4345 (3), 1879 (3)
O_2	2274
H_2O	5254, 2295, 5404
CO_2	1997, 3380, 960 (2)

TABLE A1.2

Zero Point Energy Difference between Isotopomers ($\Delta\varepsilon_0$)

Isotopomers	$\Delta\varepsilon_0$ (J mol^{-1})
CH_4/CD_4	29350
H_2O/D_2O	14910
OH^*/OD^*	5860

Therefore, the kinetic isotope effect (KIE), which is defined as the ratio of the combustion rate for CH_4/O_2 to that of CD_4/O_2, equals

$$\text{KIE} = \left(\frac{K_{3,CH_4}}{K_{3,CD_4}}\right)\left(\frac{k_{4,CH_4}}{k_{4,CD_4}}\right)\left(\frac{K_{5,CH_4}}{K_{5,CD_4}}\right). \quad [A1.6]$$

Each ratio in parentheses in Eq. [A1.6] is examined separately below.

1. $$\frac{k_{4,CH_4}}{k_{4,CD_4}} = \frac{\left(\frac{Q^{\Xi}_{CH_3{}^*OH^*}}{Q^{\Xi}_{CH_4{}^*} Q_{O^*}}\right)}{\left(\frac{Q^{\Xi}_{CD_3{}^*OD^*}}{Q^{\Xi}_{CD_4{}^*} Q_{O^*}}\right)} = \left(\frac{Q^{\Xi}_{CH_3{}^*OH^*}}{Q^{\Xi}_{CD_3{}^*OD^*}}\right)\left(\frac{Q^{\Xi}_{CD_4{}^*}}{Q^{\Xi}_{CH_4{}^*}}\right) \quad [A1.7]$$

2. $$\frac{K_{3,CH_4}}{K_{3,CD_4}} = \frac{\left(\frac{Q_{CH_4{}^*}}{Q_{CH_4} Q_*}\right)}{\left(\frac{Q_{CD_4{}^*}}{Q_{CD_4} Q_*}\right)} = \left(\frac{Q_{CH_4{}^*}}{Q_{CD_4{}^*}}\right)\left(\frac{Q_{CD_4}}{Q_{CH_4}}\right) \quad [A1.8]$$

3. $$\frac{K_{5,CH_4}}{K_{5,CD_4}} = \frac{\left(\frac{Q_{H_2O} Q_{O^*} Q_*}{Q^2_{OH^*}}\right)}{\left(\frac{Q_{D_2O} Q_{O^*} Q_*}{Q^2_{OD^*}}\right)} = \left(\frac{Q_{H_2O}}{Q_{D_2O}}\right)\left(\frac{Q_{OD^*}}{Q_{OH^*}}\right)^2 \quad [A1.9]$$

Combining Eqs. [A1.6] through [A1.9] results in

4. $$\text{KIE} = \left(\frac{Q^{\Xi}_{CH_3{}^*OH^*}}{Q^{\Xi}_{CD_3{}^*OD^*}}\right)\left(\frac{Q_{CD_4}}{Q_{CH_4}}\right)\left(\frac{Q_{H_2O}}{Q_{D_2O}}\right)\left(\frac{Q_{OD^*}}{Q_{OH^*}}\right)^2. \quad [A1.10]$$

Each ratio of the partition functions is evaluated as follows.

1. Translational partition function contribution:

$$\left(\frac{Q_{CD_4}}{Q_{CH_4}}\right)_{\text{trans}} = \left(\frac{m_{CD_4}}{m_{CH_4}}\right)^{3/2} = \left(\frac{20}{16}\right)^{3/2} = 1.398 \quad [A1.11]$$

$$\left(\frac{Q_{H_2O}}{Q_{D_2O}}\right)_{\text{trans}} = \left(\frac{m_{H_2O}}{m_{D_2O}}\right)^{3/2} = \left(\frac{18}{20}\right)^{3/2} = 0.854 \quad [A1.12]$$

The $CH_3{}^*OH^*$, $CD_3{}^*OD^*$, OH^*, and OD^* adsorbed species have zero translational degrees of freedom; the reduced masses of $CH_3{}^*OH^*$ and $CD_3{}^*OD^*$, OH^* and OD^*

adsorbed species are approximately the same. Therefore,

$$\left(\frac{Q^{\Xi}_{CH_3{}^*OH^*}}{Q^{\Xi}_{CD_3{}^*OD^*}}\right)_{trans} \approx 1 \qquad [A1.13]$$

$$\left(\frac{Q_{OD^*}}{Q_{OH^*}}\right)^2_{trans} \approx 1 \qquad [A1.14]$$

2. Rotational partition function contribution:

$$\left(\frac{Q_{CD_4}}{Q_{CH_4}}\right)_{rot} \approx (8)^{1/2} \qquad [A1.15]$$

$$\left(\frac{Q_{H_2O}}{Q_{D_2O}}\right)_{rot} \approx \left(\frac{1}{8}\right)^{1/2} \qquad [A1.16]$$

The $CH_3{}^*OH^*$, $CD_3{}^*OD^*$, OH^*, and OD^* are adsorbed species; therefore,

$$\left(\frac{Q^{\Xi}_{CH_3{}^*OH^*}}{Q^{\Xi}_{CD_3{}^*OD^*}}\right)_{rot} \approx 1 \qquad [A1.17]$$

$$\left(\frac{Q_{OD^*}}{Q_{OH^*}}\right)^2_{rot} \approx 1. \qquad [A1.18]$$

3. Vibrational partition function contribution: At low temperature, when $T < 1000$ K,

$$\left(\frac{Q_{CD_4}}{Q_{CH_4}}\right)_{vib} \approx 1 \qquad [A1.19]$$

$$\left(\frac{Q_{H_2O}}{Q_{D_2O}}\right)_{vib} \approx 1 \qquad [A1.20]$$

$$\left(\frac{Q^{\Xi}_{CH_3{}^*OH^*}}{Q^{\Xi}_{CD_3{}^*OD^*}}\right)_{vib} \approx 1 \qquad [A1.21]$$

$$\left(\frac{Q_{OD^*}}{Q_{OH^*}}\right)^2_{vib} \approx 1. \qquad [A1.22]$$

4. Electronic partition function contribution:

$$\left(\frac{Q_{CD_4}}{Q_{CH_4}}\right)_{elec} = e^{29350/RT} \qquad [A1.23]$$

$$\left(\frac{Q_{H_2O}}{Q_{D_2O}}\right)_{elec} = e^{-14910/RT} \qquad [A1.24]$$

$$\left(\frac{Q^{\Xi}_{CH_3{}^*OH^*}}{Q^{\Xi}_{CD_3{}^*OD^*}}\right)_{elec} = e^{\frac{E^{\Xi}_{CD_3{}^*OD^*} - E^{\Xi}_{CH_3{}^*OH^*}}{RT}} \qquad [A1.25]$$

$$\left(\frac{Q_{OD^*}}{Q_{OH^*}}\right)^2_{elec} = e^{11720/RT} \qquad [A1.26]$$

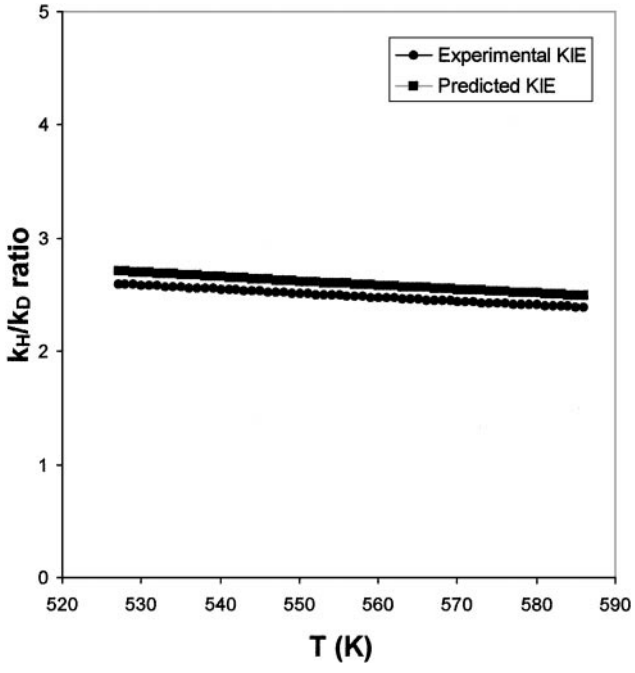

FIG. A1. Experimental and predicted results for the kinetic isotope effect.

Combining Eqs. [A1.10] through [A1.26], the kinetic isotopic effect (KIE) can be approximated as

$$\text{KIE} = 1.19e^{\frac{26160 + \left(E^{\Xi}_{CD_3{}^*OD^*} - E^{\Xi}_{CH_3{}^*OH^*}\right)}{RT}} = 1.19e^{\Delta E/RT}, \qquad [A1.27]$$

and the resulting pre-exponential factor of 1.19 is very similar to that found experimentally, 1.14. Experimental results show the ΔE is equal to 3.6 kJ/mol. Using this value the calculated zero point energy difference between transition state species $CD_3{}^*OD^*$ and $CH_3{}^*OH^*$ is 22560 J/mol. This value is a little bit smaller than that between CH_4 and CD_4 (29350 J/mol) but much larger than that between OH^* and OD^* (5860 J/mol), suggesting that the transition state species structure looks more like CH_4 and CD_4. Assuming that ΔE is equal to 3.6 kJ/mol, the predicted KIE is shown as a function of temperature in Fig. A1 along with the experimental values of the KIE.

ACKNOWLEDGMENTS

This work was supported by funds provided by the E.O. Lawrence Berkeley National Laboratory of the U.S. Department of Energy through the LDRD initiatives program.

REFERENCES

1. Burch, R., and Hayes, M. J., *J. Mol. Catal. A Chem.* **100**, 13 (1995).
2. Ribeiro, F. H., Chow, M., and Dalla Betta, R. A., *J. Catal.* **146**, 537 (1994).
3. Fujimoto, K., Ribeiro, F. H., Avalos-Borja, M., and Iglesia, E., *J. Catal.* **179**, 431 (1998).

4. Benson, J. E., Hwang, H. S., and Boudart, M., *J. Catal.* **30**, 146 (1973).
5. Lenz, D. H., and Conner, W. M. C., Jr., *Anal. Chim. Acta* **173**, 227 (1985).
6. Bird, R. B., Stewart, W. E., and Lightfoot, E. N., "Transport Phenomena." Wiley, New York, 1960.
7. Fogler, H. S., "Elements of Chemical Reaction Engineering." Prentice Hall, New York, 1992.
8. Treybal, R. E., "Mass-Transfer Operations." McGraw–Hill, New York, 1980.
9. Muller, C. A., Maciejewski, M., Koeppel, R. A., and Baiker, A., *J. Catal.* **166**, 36 (1997).
10. Au-Yeung, J., Bell, A. T., and Iglesia, E., *J. Catal.* **185**, 213 (1999).
11. Mars, P., and van Krevelen, D. W., *Chem. Eng. Sci.* **3**, 41 (1954).
12. Noggle, J. H., "Physical Chemistry." Harper Collins, New York, 1989.
13. Ozaki, A., "Isotopic Studies of Heterogeneous Catalysis." Kodansha, Tokyo, 1977.